Suprathermal electron moments in the ionosphere

Hanane Marif, Jean Lilensten

J. Space Weather Space Clim. 2020, **10**, 22

https://doi.org/10.1051/swsc/2020021

JSWSC

Available online at:
www.swsc-journal.org

RESEARCH ARTICLE OPEN ACCESS

Suprathermal electron moments in the ionosphere

Hanane Marif[1] and Jean Lilensten[2,*]

[1] Theoretical Physics Laboratory, Faculty of Physic, USTHB, B.P. 32, Bab Ezzouar, 16079 Algiers, Algeria
[2] UGA-Grenoble 1/CNRS-INSU, Institut de Planétologie et d'Astrophysique de Grenoble (IPAG), UMR 5274, Grenoble 38041, France

Received 27 November 2019 / Accepted 12 May 2020

Abstract – The ionospheric electron population is divided into two groups. The ambient electrons are thermalized. Their energy is usually smaller than one electron volt. Their densities and temperatures are the usual ones measured by incoherent scatter radars, or modeled by international codes such as International Reference Ionosphere (IRI). There is however a second population called the suprathermal electrons. This one is either due to photoionization or to electron impact between the thermosphere and the precipitation in the high latitude zone. In the frame of space weather, it may be the source of scintillations, plasma bulks and other physical phenomena. The suprathermal electron population can only indirectly be measured through the plasmaline and had never been modeled. Its modeling requires the computation of the electron stationary flux by solving the Boltzmann transport equation. This flux is multiplied by various powers of the velocity v and integrated to obtain the different order moments. By integrating f over $v^0 \mathrm{d}v$, one deduces the suprathermal electron density. An integration of $v^1 f \mathrm{d}v$ allows the computation of their mean velocity. Higher moments give access to their temperature and finally to their heat flux. In this work, we demonstrate for the first time the full and rigorous calculation of the ionospheric electron moments up to three. As two case studies, we focus on high latitude in the auroral oval and low magnetic latitude over Algiers for different solar and geophysical conditions. We compare the suprathermal densities and temperatures to the thermal electron parameters. Our results highlight that – as expected – the suprathermal density is small compared to the thermal one. Although it is close to 3×10^3 m^{-3} at 180 km during the day, it drops drastically at night, to hardly reach 3 m^{-3}. Contrarily to the density, the velocity is about 10 times more important during the nighttime when precipitation occurs than during the daytime under the electromagnetic solar flux. At 400 km, it varies during the day between 700,000 m s^{-1} (active solar conditions) and 900,000 m s^{-1} (quiet Sun). At night, the velocity varies between 3×10^6 m s^{-1} (low mean energy precipitation) and 3×10^7 m s^{-1} (high mean energy precipitation) at 400 km. The suprathermal temperature increases as the solar activity decreases or as the mean energy of the electron precipitation increases. It may reach values close to 3×10^8 K. The heat flux may be fully oriented downward or experiences a reversal with some flux going up depending on the forcing.

Keywords: Thermosphere / Ionosphere / Suprathermal particle / Boltzmann moments

1 Introduction

Many textbooks present the ionosphere in detail. A full description is therefore out of scope of this work. Even a full bibliography would be impossible to provide. We recommend for example Rees (1989) for a complete description of the upper atmosphere and we cite some other books in this article. However, there are still sometimes an ambiguity in the phrasing. The *thermosphere* is the neutral part of the atmosphere above typically 75–80 km, mainly composed of N_2, O_2 and O up to about 500 km; the *ionosphere* is the ionized part composed of electrons and ions. The *upper atmosphere* is the merging of the two. In the ionosphere, the electrons may be sub-divided into two distinct populations.

The thermal electrons constitute the main electron population. It may be considered as a fluid. Several of its macroscopic parameters (density, velocity, temperatures) are measurable through different means such as including the ionosondes or the incoherent scatter radars. These parameters are heavily modeled, the main international model being IRI (Bilitza et al., 2012). The energy of these electrons is typically of the order of the electron-volt with a Maxwellian distribution.

The second population is called the suprathermal electrons. Its energy spectrum has characteristic energies larger than the

*Corresponding author: jean.lilensten@univ-grenoble-alpes.fr

thermal population, up to several keV. It originates in two main sources:

- Photoproduction: the EUV flux energy is higher than typically 10 eV, i.e. the order of the ionization energy threshold for all the molecular and atomic atmospheric species. After a photoionization, the extracted electron, called primary photo-electron, has a kinetic energy equal to the difference between the incident beam and the ionization threshold. Since the EUV energy can be as high as 350 eV, the created electron is often energetic enough to create secondary ionization through collisions. The primary photo-electron production due to the EUV interaction can be accurately described with a Beer-Lambert law (again, this is described in many textbooks such as Rees, 1989). The dynamics of this primary photo-electron population is driven by the fluid mechanics. They mainly follow the neutral wind, with an additional diffusion factor. The electrons are linked to the ion population through the Laplace force, so that the plasma is globally neutral (Kelley, 2009).
- Electron precipitation (Banks & Kockarts, 1973): they occur mainly at high latitude in the auroral oval, but can also occur in the polar cusp. The energy of the precipitated electrons is highly variable and ranges from a few tens of eV to MeV. They are therefore an important source of atmospheric ionization. In this case, the precipitation is the primary source while the electrons created through collision impacts are the secondary electron population. Due to the magnetic mirroring, the precipitated ions (mainly protons) are usually stopped above 500 km while the electrons can go down along the magnetic field lines to about 80 km, depending on their initial energy and pitch angle (Lummerzheim et al., 1989). This charge separation is at the origin of field aligned currents that are out of the scope of this paper.

The macroscopic characteristics of this suprathermal population has never been investigated. It is clear from different studies (i.e. Min et al., 1993) or textbooks such as Woods (1993) that they are in small numbers compared to the thermal ones and that their density, velocity or temperature play little role on the global characteristics of the ionospheric plasma. However, they are still a component of our space environment and are worth exploring. Moreover, they are important in order for example to understand the plasmaline (Kofman et al., 1993; Guio et al., 1998; Guio & Lilensten, 1999). They may also play some role in the creation of blobs or patches at the origin of the space weather mechanism of scintillation at high (Jin et al., 2018) or low latitudes (Blanch et al., 2018).

We present here a first calculation of the macroscopic parameters of this suprathermal electron population based on the suprathermal velocity distribution function derived from the stationary flux calculated by an electron kinetic transport model. We show their first moments (order 0–3) and compare them to the thermal parameters in two different geophysical conditions at two different latitudes and under the two different sources (solar electromagnetic flux and precipitation).

2 Mathematical model

2.1 The Boltzmann kinetic equation

The computation of the suprathermal moments requires to know the stationary electron flux. It can be computed by solving the stationary kinetic Boltzmann transport equation. The computer program solving this equation along the magnetic field line with complete references concerning the cross sections used in the model are described in detail in Lummerzheim & Lilensten (1994); Lilensten & Blelly (2002); Lilensten et al. (2013), and will not be repeated here. We only describe hereafter the philosophy of the code.

The vertical stationary kinetic transport equation expresses the fact that the variation of the steady state electron flux with the scattering depth at a given altitude, energy and pitch angle, is the difference between what leaves that energy, altitude or angle slab and what enters it (i.e. Strickland et al., 1976; Basu et al., 1993). It describes the angular and energy redistributions of the electrons flux from the top of the ionosphere to the low E region. Its unknown is the stationary electron flux ϕ (in $\mathrm{cm}^{-2}\ \mathrm{s}^{-1}\ \mathrm{eV}^{-1}\ \mathrm{sr}^{-1}$) which depends on the altitude z, the electron energy E and pitch angle θ relative to the magnetic field. However, in the literature, the pertinent angle parameter is $\mu = \cos(\theta)$.

This equation can be solved under the following assumptions: first, we assume that electrons are predominantly transported along magnetic field lines. Secondly, the motion of the electrons is represented by the motion of their center of gyration along the magnetic field. The effect of ionospheric horizontal electric fields on the energetic electrons is small and is neglected. The acceleration of the electrons is assumed to have taken place above the modeled altitude range, and local field aligned potential drops and the mirror force from the converging geomagnetic field are neglected. Finally, we can assume the stationary state for the kinetic transport. The main reason is that the time of the absorption of the suprathermal particles by the atmosphere is much smaller than the changes in the source of those particles: the typical collision frequencies are of the order of one per second, while the precipitation occur over several seconds to several hours, and the photoelectron production varies in a significant manner over a few minutes, when the Earth rotates. Therefore, the stationary assumption means that any time a suprathermal particle is absorbed, another one with the same characteristics (in term of energy and pitch angle) is created. Of course, that also means that the kinetic equation must be solved again any time the external conditions change, for example any time the precipitating flux changes at the top of the atmosphere. This is of great importance for time depending analysis, such as the coupling of the kinetic and fluid approaches (Blelly et al., 2010; Pitout et al., 2013). Finally, we obtain a suprathermal electron flux a function of energy, pitch angle and time.

During an ionization process, the incident electron called primary electron is scattered mostly forward, whereas the extracted electron called secondary electron may be scattered into any direction (Opal et al., 1971).

Variations in energy or angle due to collisions are described through differential cross sections, deduced from the total cross sections as described in Culot et al. (2005), and updated in

Lilensten et al. (2013). Energy loss also occurs from the heating of the ambient thermal electron gas due to suprathermal hot electrons to thermal electrons interactions. This loss comes from the combined effects of two body Coulomb collisions and the collective effect of Cerenkov emission of plasma waves. Mantas (1975) treated this loss process as an extra "friction" term, assuming a continuous energy loss of the hot electrons to the ambient electrons, without any deflection during the process. In the literature, this approximation is referred as "the continuous flowing down approximation" (Swartz & Nisbet, 1972; Swartz, 1985). This mechanism describes how the suprathermal electrons and the thermal ones friction against each other. It is only efficient if the suprathermal go slowly enough, i.e. in term of energy, below 10 eV, and still more below 5 eV. Therefore, this friction does not influence the electron production through collision with the thermosphere because all the ionization thresholds in the Earth atmosphere are larger than 10 eV. This friction depends also on the thermal electrons characteristics, i.e. on their density N_e and temperature T_e. This is the only place where these parameters may be influential. In the following of this work, we will often refer to N_e and T_e in order to compare their values to the suprathermal ones. At all stage, it will be important to keep in mind that they play no role on the suprathermal parameters.

The algorithm solving the penetration and scattering equation is a discrete ordinate method reviewed by Stamnes et al. (1988). The first version of this code is described in Lummerzheim & Lilensten (1994). Since then, it has been constantly improved and used in different applications. A more recent description is given in Lilensten & Cander (2003) and the latest developments are in Lilensten et al. (2013).

The main inputs of this model are the neutral atmosphere, the electron temperature and density profiles, the electron impact cross sections The full bibliography for the cross sections is given in Lilensten & Cander (2003). The neutral atmosphere is provided by the empirical model NRLMSISE-00, (Picone et al., 2002). The electron temperature and density profiles are given by the IRI model (Bilitza et al., 2012).

During the nighttime, the flux of precipitating electrons at the top of the ionosphere is an additional input of the model. Following Rees (1989), we impose a flux of precipitating electrons made of two components: a Maxwellian centered at a suprathermal energy E_o (typically a few keV) and a power law below 10 eV. This flux enters the upper atmosphere with a given pitch angle distribution. The bulk of the particles are directed along the local magnetic field line. The flux of particles decreases gradually from this parallel direction and becomes zero in the direction perpendicular to the magnetic field. Only the mean energy (peak E_o) of the Maxwellian and the total integrated energy (E_{tot}) are free parameters.

During the daytime, the EUV flux is taken from the Solar Spectral Irradiance Reference Spectra for Whole Heliosphere Interval (WHI) model (Woods et al., 2009). The primary photo-electron production due to the EUV flux can then be accurately described with a Beer-Lambert law. The inputs are the photoabsorption cross sections, which are summarized in (Lilensten & Cander, 2003; Lilensten et al., 2013). The main outputs are the energy deposited at each altitude by the solar irradiance at any wavelength through ionisation and excitation, and the excitation and ionisation productions, called "Primary production", in $cm^{-3}\ s^{-1}$.

2.2 The suprathermal moments

Once the distribution function ϕ is computed, it is possible to deduce the suprathermal parameters by integrating ϕ over different powers of the velocity v. Again, several textbooks describe this process in term of the velocity and position parameters. We can recommend as examples (Lilensten & Blelly, 2000; Schunk & Nagy, 2000; Bittencourt, 2010). However, these developments were always provided in term of the usual parameter, i.e. the vector position and the vector velocity. In the ionosphere, these parameter reduce to the altitude, the energy and the pitch angle z, E, ϕ. Several attempts were made to adapt the fluid equations to the ionospheric conditions (i.e. Akasofu & Chapman, 1972; Schunk & Nagy, 2000). However, an initial error in the mathematics (with an unknown origin) propagated through the literature, preventing a correct solution. A more complete approach with application to the plasma line was provided in Guio et al. (1998) where the first order moments (0 and 1) were computed. We provide here the complete solutions for the moments up to 3. Two demonstrations of the suprathermal moments are provided in the appendix. We only provide the final formula in the main text.

Classically, the Boltzmann distribution function (in $cm^{-6}\ s^3$) is $f(t,\vec{r},\vec{v})$. The particle velocity is $\vec{v}$ which is splitted in velocities parallel and perpendicular to the magnetic field line $\vec{v} = v_{//}\vec{i_{//}} + v_\perp \vec{i_\perp}$. We make the stationary hypothesis. The electrons are gyrating along the magnetic field that we call the z axis, so that the Boltzmann distribution function $f(t,\vec{r},\vec{v})$ (in $cm^{-6}\ s^3$) can be simply expressed as $f(z, v_\perp, v_{//})$. It can also be expressed as a function of the suprathermal electrons stationary flux $\phi(z,E,\mu)$ ($cm^{-2}\ eV^{-1}\ s^{-1}\ sr^{-1}$) solution of the Boltzmann transport equation through:

$$f(z, v_\perp, v_{//}) = \frac{m^2}{2E}\phi(z,E,\mu) \tag{1}$$

and

$$2\pi v_\perp \mathrm{d}v_\perp \mathrm{d}v_{//} = 2\pi\sqrt{\frac{2E}{m^3}}\,\mathrm{d}\mu\,\mathrm{d}E \tag{2}$$

$\mu = \cos(\theta)$ and θ is the angle between the magnetic field line and the electron trajectory (usually also called "pitch angle"), $E = \frac{1}{2}mv^2$ is the non-relativistic electrons kinetic energy. m is the electron mass.

Zeroth order moment: the suprathermal electron density (in m^{-3})

$$\begin{aligned} n(z) &= \int f(z,v)\mathrm{d}v = \iint f(z, v_\perp, v_{//}) 2\pi v_\perp \mathrm{d}v_\perp \mathrm{d}v_{//} \\ &= 2\pi \iint \sqrt{\frac{m}{2E}}\phi(z,E,\mu)\,\mathrm{d}\mu\,\mathrm{d}E. \end{aligned} \tag{3}$$

This moment allows to define a distribution function from which one can compute the average $\langle X \rangle$ of any random variable X as:

$$\langle X \rangle = \frac{1}{n(z)} \int X f(z, v_\perp, v_{//}) 2\pi v_\perp \mathrm{d}v_\perp \mathrm{d}v_{//} \tag{4}$$

and transform it in the (μ, E) frame using equations (1) and (2). For more details see Appendixes A and B.

First order moment: the suprathermal electron velocity (in cm s^{-1})

We note that over a full rotation, the average of the perpendicular velocity is null, so that $\langle v\rangle = \langle v_{//}\rangle$:

$$\langle v(z)\rangle = \langle v_{//(z)}\rangle = \frac{1}{n(z)}\int v_{//(z)} f(z, v_\perp, v_{//}) 2\pi v_\perp \mathrm{d}v_\perp \mathrm{d}v_{//} = 2\pi \frac{1}{n(z)} \iint \phi(z, E, \mu)\mu \ \mathrm{d}\mu \, \mathrm{d}E. \quad (5)$$

Second order moment: the suprathermal electron temperature (in K)

The instantaneous velocity $\vec{v}$ of the suprathermal electrons may be divided in the mean velocity $\langle\vec{v}\rangle$ along B, in relation to the overall or drift motion of the electrons, computed in equation (5) and specific velocity $\vec{c}$ depending on each electron agitating energy: $\vec{c} = \vec{v} - \langle\vec{v}\rangle$. To compute the suprathermal electron temperature (in K), we use the thermodynamic definition of the kinetic temperature $\frac{3}{2}kT = \frac{1}{2}m\langle c^2\rangle$ where k is the Boltzmann constant.

So

$$\frac{3}{2}kT = \frac{1}{2}m\left(\langle v^2\rangle - \langle v\rangle^2\right). \quad (6)$$

So that

$$\frac{3}{2}kT = \frac{m}{2n(z)}\int v^2 f(z, v_\perp, v_{//}) 2\pi v_\perp \mathrm{d}v_\perp \mathrm{d}v_{//} - \frac{m\langle v\rangle^2}{2} \quad (7)$$

which becomes:

$$\frac{3}{2}kT = 2\pi\frac{1}{n(z)}\iint \sqrt{\frac{mE}{2}}\phi(z, E, \mu)\,\mathrm{d}\mu\,\mathrm{d}E - \frac{m\langle v\rangle^2}{2}. \quad (8)$$

Equation (8) allows to define three temperatures. The total temperature T_{tot} in relation to the instantaneous velocity, the specific or kinetic one $T = T_{\mathrm{spec}}$ and the mean one T_{mean}:

$$T_{\mathrm{tot}}(z) = \frac{2\pi}{3k}\frac{1}{n(z)}\iint \sqrt{2mE}\,\phi\,(z, E, \mu)\,\mathrm{d}\mu\,\mathrm{d}E \quad (9)$$

$$T_{\mathrm{mean}}(z) = \frac{m}{3k}\langle v_{//}\rangle^2 \quad (10)$$

where $\langle v\rangle = \langle v_{//}\rangle$ and:

$$\begin{cases} T_{\mathrm{spec}}(z) = T_{\mathrm{tot}}(z) - T_{\mathrm{mean}}(z) \\ \quad = \frac{2\pi}{3k}\frac{1}{n(z)}\iint \sqrt{2mE}\,\phi\,(z, E, \mu)\,\mathrm{d}\mu\,\mathrm{d}E - \frac{m\langle v_{//}\rangle^2}{3k}. \end{cases} \quad (11)$$

Third order moment: the supra thermal electron heat flow (in $eVm^{-2}\ s^{-1}$)

$$\vec{q}(z) = \frac{1}{2}n(z)\ mc^2\vec{c}. \quad (12)$$

The suprathermal heat flow is the projection of $\vec{q}(z)$ parallel to the magnetic field line. We call it $\chi(z)$. Developing $\vec{q}(z)$, we obtain:

$$\chi(z) = \langle q_{//}(z)\rangle = \chi_1(z) + \chi_2(z) + \chi_3(z) + \chi_4(z) + \chi_5(z) \quad (13)$$

where:

$$\begin{cases} \chi_1(z) = \int E\phi_1(z, E)\ \ \mathrm{d}E \\ \chi_2(z) = -\langle v\rangle\int \phi_0(z, E)\sqrt{\frac{mE}{2}}\ \ \mathrm{d}E \\ \chi_3(z) = \frac{3}{2}m\langle v\rangle^2\int \phi_1(z, E)\ \ \mathrm{d}E \\ \chi_4(z) = -\langle v\rangle^3\sqrt{\frac{m^3}{8}}\int \frac{1}{\sqrt{E}}\phi_0(z, E)\ \ \mathrm{d}E \\ \chi_5(z) = -\langle v\rangle\int \phi_2(z, E)\sqrt{2mE}\ \ \mathrm{d}E \end{cases} \quad (14)$$

where $\phi_j(z, E) = 2\pi\int \mu^j\phi(z, E, \mu)\,\mathrm{d}\mu$ and $j = 0$, 1, or 2.

3 Results

The number of geophysical cases is so huge that a detailed study of the suprathermal moments at all geographical locations, all solar conditions and all geomagnetic conditions makes simply no sense. We chose to provide here few typical cases. The effect of the solar electromagnetic flux will be studied over Algiers (Latitude = 36.75°, longitude = 3.04°) at local noon. The effect of the nightside electron precipitation will be provided above the EISCAT radar near Tromsø (Latitude = 69.58°, longitude = 19.23°). We will explore different solar and geomagnetic activity conditions.

3.1 Dayside case: Detailed study over Algiers during quiet solar and geomagnetic conditions

The first case corresponds to a decimetric index $F10.7 = 80$, i.e. a quiet sun at noon. The main parameter for the thermosphere and the ionosphere is however the average of $F10.7$ over the previous days. The models take a summation over 81 days. Here, we impose that this average is equal to the daily value in order to avoid confusion. In the following, the term $F10.7$ will therefore designate indifferently the daily or the average value. The geomagnetic activity is $Ap = 3$, i.e. a quiet condition as well. The neutral atmosphere is given in Figure 1. There is no commentary to make on this figure since it presents the classical features of a quiet low latitude thermosphere with an exospheric temperature of about 800 K.

As described above, the solar flux penetrates in this atmosphere. It is absorbed through photoexcitation and photoionization. The input solar electromagnetic flux comes from Woods et al. (2009) ranging from 0.05 nm up to 2400 nm. However, the wavelengths that are efficient to ionize or excite the thermosphere range from 2.45 nm (506.04 eV) to 103.15 nm (12.02 eV), i.e. the extreme UV to XUV. Figure 2 shows the altitude where it is absorbed at all wavelengths (Solar Spectrum Irradiance, or SSI) and its integral over the wavelengths at all altitudes (Total Solar Irradiance, or TSI). We recall that the SSI and the TSI were calculated by the model described in Section 2.1. Here again, the depositions is not uniform. It depends on the different cross sections of each atom or molecule encountered at each wavelength. Above 300 km, the absorption remains small (about 1% of the total energy).

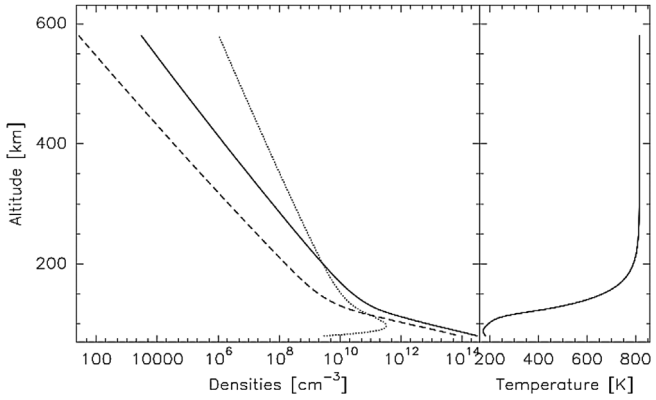

Fig. 1. Left panel: Neutral densities (MSIS, Picone et al., 2002) over Algiers ($F10.7$ = 80, Ap = 3). Full line: N_2, dotted line: O, dashed line O_2. Right panel: Neutral temperature.

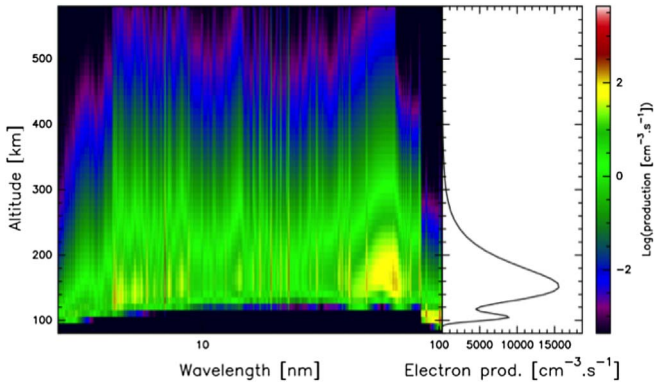

Fig. 3. The left panel shows the logarithm of the primary electron production (cm^{-2} s^{-1}) as a function of the total solar irradiance wavelength (nm) and the altitude (with the color code in the scale on the right side). The right panel is the integration over all wavelenghts.

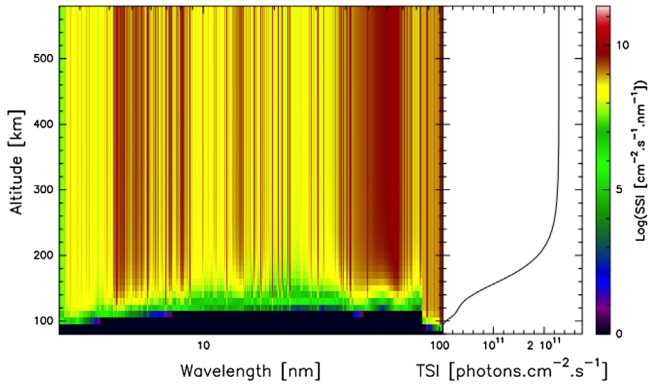

Fig. 2. The left panel shows the logarithm of the Solar Spectrum Irradiance, or SSI (cm^{-2} s^{-1} nm^{-1}) as a function of the wavelength (nm) and the altitude. The color code lies in the right of the figure. The right panel is the integration over all wavelengths (Total Solar Irradiance, or TSI).

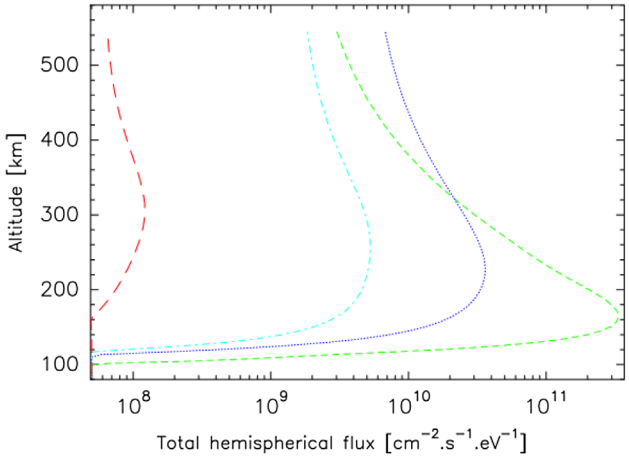

Fig. 4. Hemispheric stationary flux deduced from the kinetic Boltzmann equation integrated over all the angles. Green: 1 eV; dark blue: 10 eV; light blue: 20 eV; red: 50 eV.

The solar flux photoionization creates a primary production (Fig. 3). This production varies with the wavelength as a function of the different photoabsorption cross sections. At low altitude, this primary photoproduction is not only due to high energy photons (i.e. low wavelengths) but the low energy photons also play an important role in it. This is due to the fact that the ionization cross sections are larger close to the ionization threshold. Not surprisingly, this is the origin of the E and F ionospheric regions clearly seen in this figure around 90 and 160 km.

This primary photoproduction will then collide with the ambient gas to create a secondary production. The kinetic transport equation provides the stationary electron flux ϕ (in cm^{-2} s^{-1} eV^{-1} sr^{-1}). Figure 4 shows some profiles integrated over all the pitch angles (and called total hemispherical flux; total meaning the sum of upward and downward fluxes) at four different energies. This flux decreases rapidly with the electron energy, so that we do not provide the upper energy ones (i.e. 507 eV in our dayside computation, corresponding to the largest energy in the input solar flux). This decrease is simply a result of the fact that most of the high energy electrons lose their energy through collisions to create more low energy ones.

The fluid moments are direct outputs of this electron flux. Figure 5 shows the moments up to three over Algiers at low solar and geomagnetic activities. The temperatures and densities are compared to that of the thermal ones. Not surprisingly, the suprathermal electron density is smaller than that of the thermal one by a factor of 10 (at 180 km) to 100 (at 600 km) which is in perfect agreement with Min et al. (1993) and Woods (1993). Their detection remains therefore a challenge for the future, and only the measurement of the plasma line may give some hints about them (Guio & Lilensten, 1999). We will see that the case is still less favorable during nightside conditions. Their velocity is large, up to 800 kms^{-1} at 600 km (where there are however less than 1000 suprathermal electrons per cubic meter). Since the temperature is the next moment after the velocity, this high velocity implies a temperature much larger than that of the thermal electrons. Indeed, IRI gives a thermal electron temperature up to about 2460 K at 600 km while the suprathermal electron temperature is equal to 46,400 K at the same altitude.

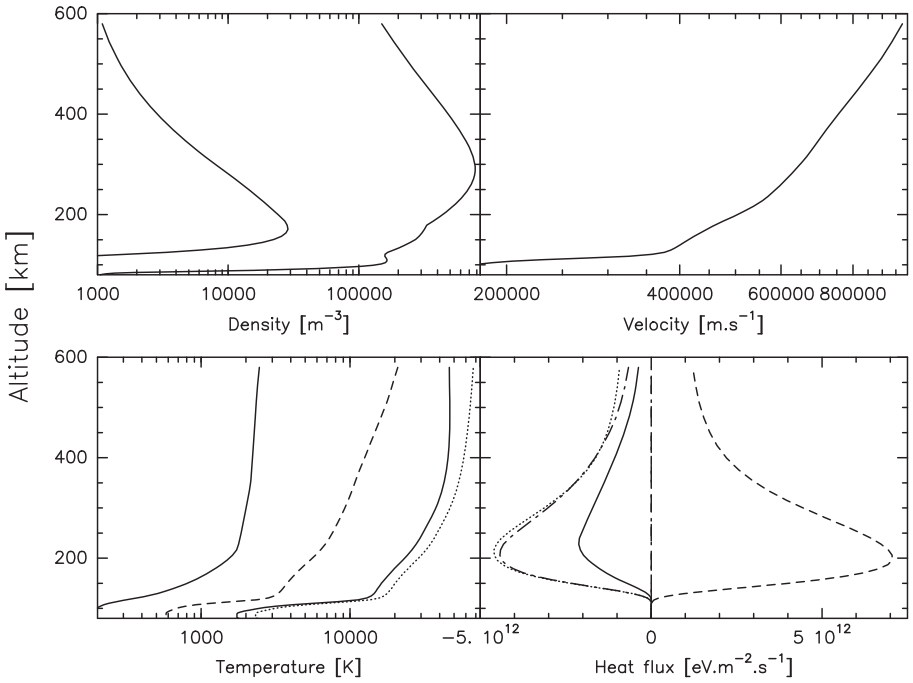

Fig. 5. Suprathermal moments over Algiers during daytime. Upper left panel: from left to right, suprathermal electron density computed in this work, compared to the thermal one provided by IRI (Bilitza et al., 2012). Right panel: suprathermal velocity. Lower left pannel: from left to right, thermal electron temperature provided by IRI, suprathermal electron temperature (dashed line: mean temperature; full line: specific temperature; dotted line: total suprathermal electron temperature). Right panel: suprathermal heat flux. With respect to equation (13), we have from left to right: $\chi_2(z)$ in dotted line, $\chi_5(z)$ in dot-dashed line, full line $\chi(z)$, along the 0 abscissa are $\chi_3(z)$ and $\chi_4(z)$ which are negligible at this scale compared to the other quantities, and finally on the right side is $\chi_1(z)$ in dashed line. The velocity and the heat fluxes are positive downward.

This temperature is the difference between two terms with respect to equation (11). The most important one remains the specific temperature $T_{spec}(z)$ which maximises at 67,300 K at the upper atmosphere considered here. However, the mean temperature $T_{mean}(z)$ is far from being negligible with a maximum value equal to 20,900 K. This component decreases with the altitude as the electron velocity decreases, but always remains far above the thermal electron temperature. The heat flux is positive downward. The main component is $\chi_1(z)$ with respect to equation (13). It is oriented downward. However, amongst the other components, $\chi_2(z)$ and $\chi_5(z)$ oriented upward largely balance it so that the sum is upward, reflecting the fact that the heat goes from the hotter to the colder electrons. The other components ($\chi_3(z)$ and $\chi_4(z)$) are smaller than 10^{-3} eVcm^{-2} s^{-1}, i.e. negligible.

3.2 Dayside case: Comparison of different solar and geomagnetic conditions over Algiers

We do not need to study in detail all the parameters shown above to perform this comparison. The test case above was for a decimetric index $F10.7 = 80$, i.e. a quiet sun at noon and a geomagnetic activity index of $Ap = 3$, i.e. a quiet condition as well. Here, we keep the Ap index equal to 3 while the solar activity index is successively equal to 120 (mid) and 200 (active). Finally, we also vary Ap for extreme geophysical conditions ($Ap = 300$), but in order to allow a comparison with the test case, we keep the solar activity $F10.7 = 80$. These parameters change the solar irradiance (F10.7), the thermosphere given by MSIS through both $F10.7$ and Ap and the electron (and ion) temperature(s) provided by IRI through $F10.7$ only (in IRI, Ap only influences the auroral oval model). Because the thermal electron temperature and density have little influence on the Boltzmann equation, we do not try to define them precisely and will use IRI in the standard mode (there are many switches in this model allowing different considerations on the external forcings). Note that the electron density in this standard mode of IRI depends on the time and the day, but not on $F10.7$, and will therefore remain constant in the current study. In order to show this variability, we provide the ionosphere and thermosphere parameters in Figure 6.

The process described above is ran in all different cases. In Figure 7, we only show the total suprathermal heat flux and the total suprathermal temperature and not their different components, as the behavior is similar to the study in Section 3.1.

The variation of the suprathermal parameters closely follows that of the neutral density. At low altitude (below about 180 km), the thermosphere experiences slight variations through N_2 and O_2. Above this altitude, these molecules vary as shown in Figure 6 but the atomic oxygen which becomes preponderant is also more variable. Therefore the larger variability of the electron stationary flux and then of the suprathermal moments. The suprathermal electron density may be multiplied by a factor of 5 at 600 km when the solar/geomagnetic activity increases.

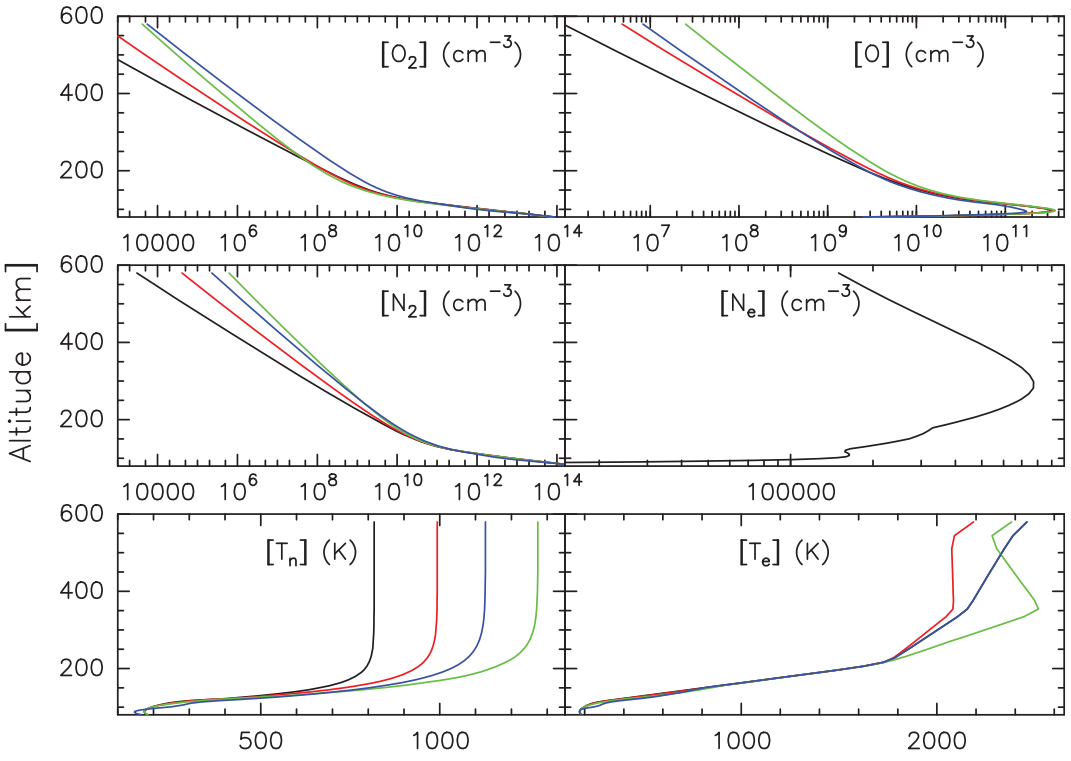

Fig. 6. The four cases under study. The color code is: $F10.7 = 80$, $Ap = 3$ (black), $F10.7 = 120$, $Ap = 3$ (red), $F10.7 = 200$, $Ap = 3$ (green) and $F10.7 = 80$, $Ap = 300$ (blue). Variation of the O_2 density (upper left), O (upper right), N_2 (middle left) and electron density (middle right). Bottom panels: Neutral temperature (left) and electron temperature (right). Since the values provided by IRI only depend on $F10.7$ and not on Ap, the blue and the black lines are superposed in the temperature and electron density curves.

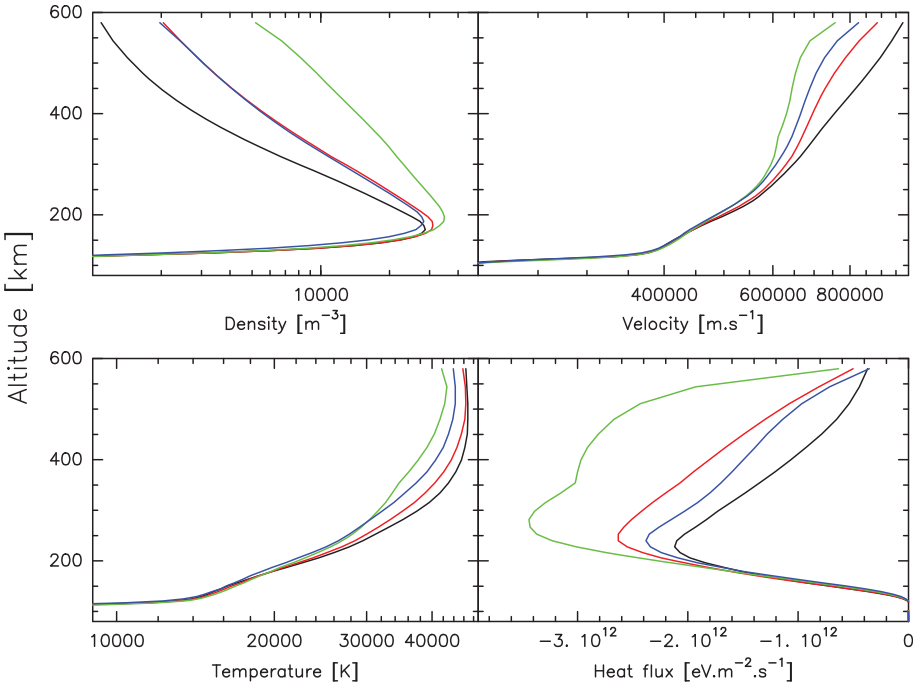

Fig. 7. Suprathermal moments for the four cases under study. As in Figure 6, the color code is: $F10.7 = 80$, $Ap = 3$ (black), $F10.7 = 120$, $Ap = 3$ (red), $F10.7 = 200$, $Ap = 3$ (green) and $F10.7 = 80$, $Ap = 300$ (blue).

As 4this density increases, the other parameters decrease since they depend on the inverse of the suprathermal electron density. The velocity decreases by a factor of about a quarter at the upper altitude (9.75×10^5 m s^{-1} in the quiet test case down to 7.57×10^5 m s^{-1}). The effect is smaller on their temperature (about 10% at 600 km). The maximum variability in the heat flux occurs between about 220 km and 550 km where the value is almost divided by a factor of 2.

3.3 Nightside case: over Tromsø in the auroral oval

Since the influence of neutral atmosphere on the suprathermal moments was studied in Section 3.2, we will now study the effect of the precipitations in the auroral oval. In this aim, we maintain the same geophysical conditions (Ap = 120) and solar ones ($F10.7$ = 80). We chose arbitrarily to place the study the 1st of January, 2015 at 22 LT, in order to have no influence of the solar electromagnetic flux. Rees (1989) mentions that the electron precipitations may be considered as the sum of a power low at low energy and a Maxwellian with a mean energy E_o. E_{tot} is the total energy carried by the precipitating initial flux at the upper atmosphere. It is the sum of all the energies. The stationary assumption implies that this does not depend on the time: E_{tot} represents the energy at time considered for the run (e.g. Jasperse, 1976). A good order of magnitude to keep in mind is that E_{tot} = 1 erg corresponds to a faint visible aurora. This energy unit is rarely used, except in this precise case because of this consideration (1 erg = 6.2415×10^{11} eV). Other studies such as Hardy et al. (1985) contradict this electron precipitation shape. However, in front of the multiplicity of cases, we will keep Rees' s formulation. In Figure 8, we show such a spectrum for a mean energy E_o = 500 eV and a total energy E_{tot} = 5 erg.

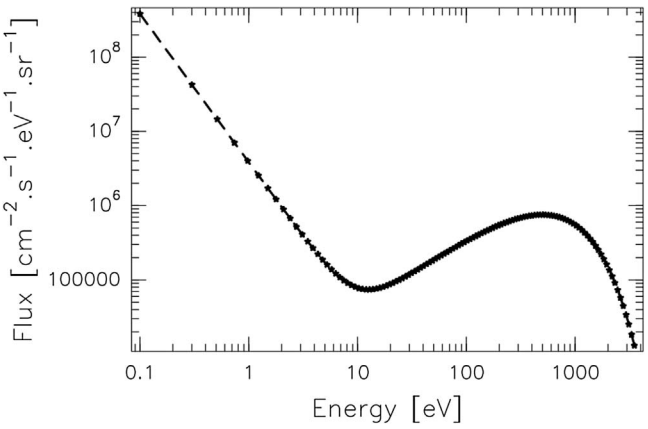

Fig. 8. Electron precipitations for a mean energy E_o = 500 eV and a total energy E_{tot} = 5 erg.

With this atmosphere and this precipitation, we obtain the moments provided in Figure 9.

The first prominent feature is the very small value of the suprathermal electron density, which is divided by a factor larger than 1000 compared to the low latitude midday. This makes their detection still more challenging for the future than

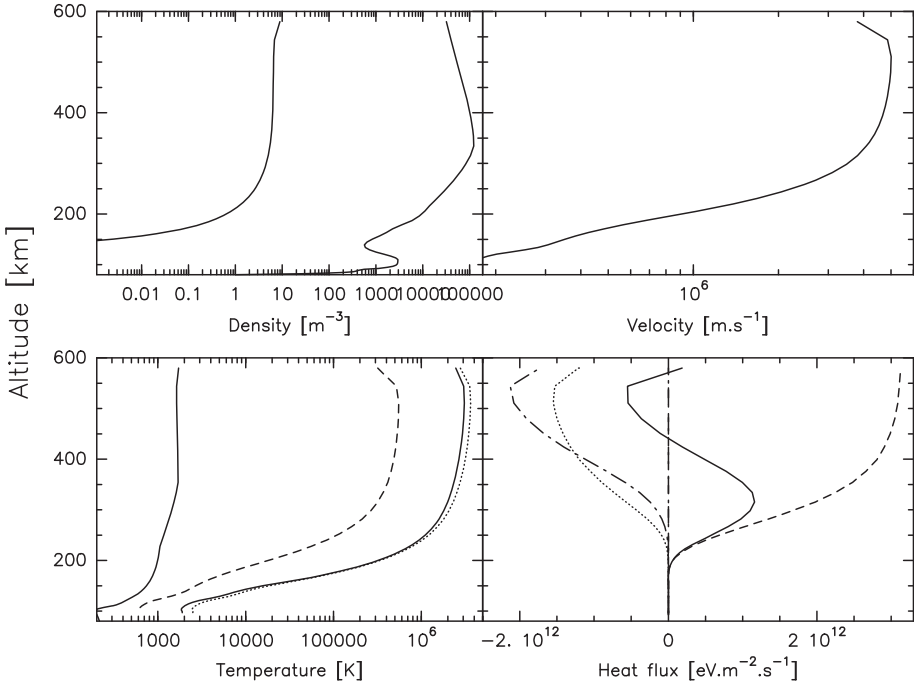

Fig. 9. Suprathermal moments in the auroral oval during nighttime. Upper left panel: from left to right, suprathermal electron density computed in this work, compared to the thermal one provided by IRI (Bilitza et al., 2012). Right panel: suprathermal velocity. Lower left pannel: from left to right, thermal electron temperature provided by IRI, suprathermal electron temperature (dashed line: mean temperature; full line: specific temperature; dotted line: total suprathermal electron temperature). Right panel: suprathermal heat flux. With respect to equation (13), we have from left to right: $\chi_2(z)$ in dotted line, $\chi_5(z)$ in dot-dashed line, full line $\chi(z)$, along the 0 abscissa are $\chi_3(z)$ and $\chi_4(z)$ which are negligible at this scale compared to the other quantities, and finally on the right side is $\chi_1(z)$ in dashed line. The velocity and the heat fluxes are positive downward.

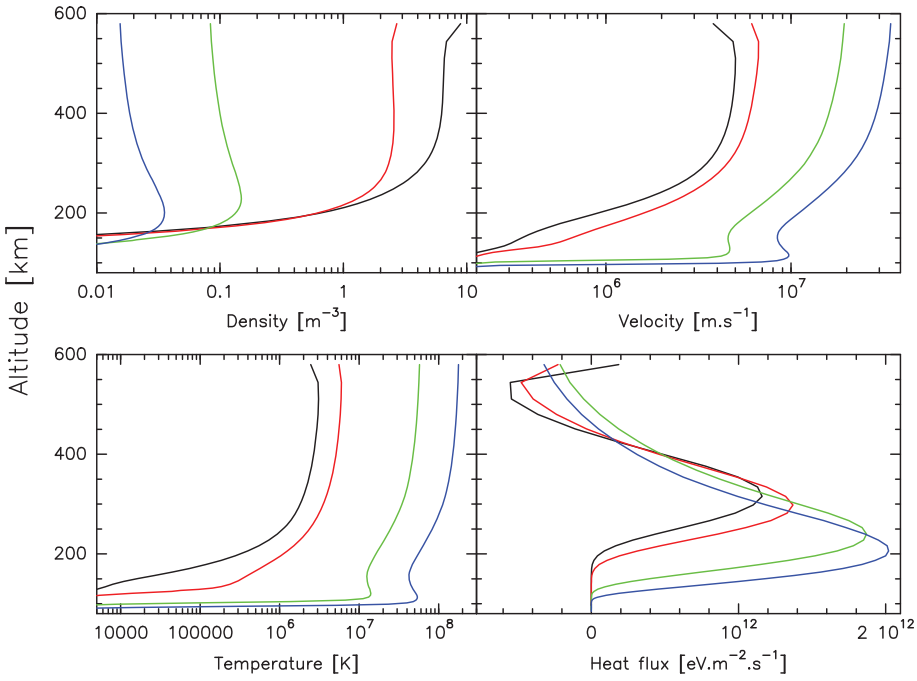

Fig. 10. Electron moments for a mean energy E_o = 500 eV (black), 1 keV (red), 10 keV (green) and 100 keV (blue) and a similar total energy E_{tot} = 5 erg.

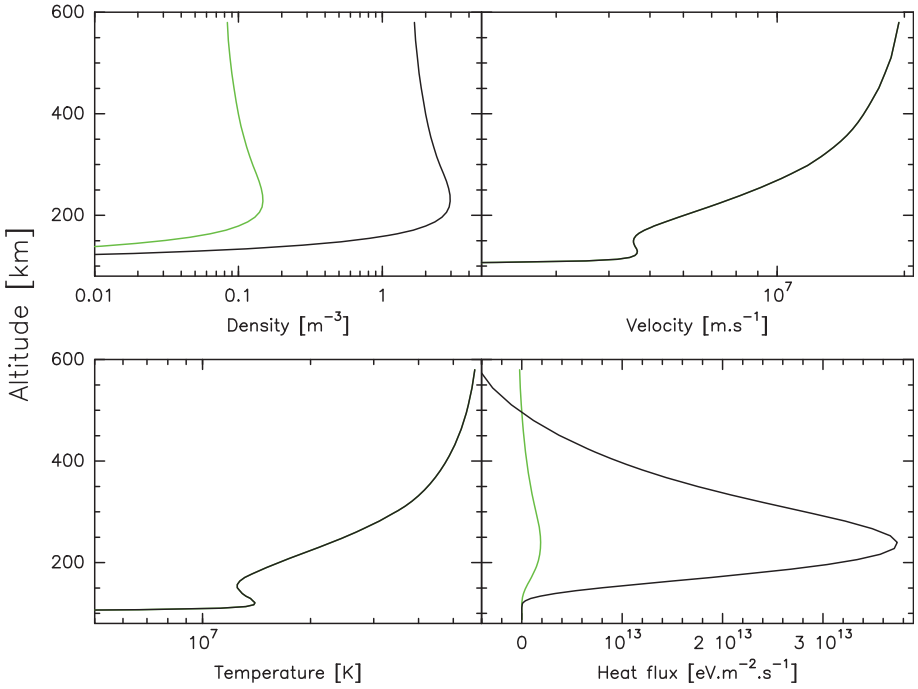

Fig. 11. Electron moments for a total energy E_{tot} = 5 erg (green) and 100 erg (black) and a similar central energy E_o = 10 keV.

during the day. The velocity though is much larger, reaching 5×10^6 m s^{-1}. The suprathermal electron temperature becomes tremendous with values above the million Kelvins. Although of the same order of magnitude than during the day, the heat flux is more variable, with downward oriented slabs (below approximately 400 km) and upward ones (above), reflecting the inversion of the electron suprathermal velocity. But considering the small amount of suprathermal electrons (about 10^5 times less than the thermal ones), these impressive characteristics hardly have any influence on the global behavior of the upper atmosphere.

In Figure 10, we show the variability of the suprathermal electron moments when the center energy E_o varies while the total energy remains constant (E_{tot} = 5 erg).

The counterpart (E_o constant at 10 keV and different E_{tot}) is shown in Figure 11.

The effect of the central energy is dramatic. The density may be divided by a factor of 100 between 500 eV and 100 keV. The important feature is that this ratio is maintained approximately at all the altitudes above 220 km. The higher the central energy, the deeper the electrons can penetrate into the upper atmosphere. Therefore, the suprathermal electrons still exist at 120 km when E_o is large while there are no longer any of them when E_o is small. As in the case of the dayside suprathermal moments, the effect is inverted on the velocity and the temperature. The former reaches values as high as 3×10^7 m s^{-1}, i.e. still two order of magnitude below the light velocity (justifying the assumption that these particles are not relativistic). The temperature reaches about 200 million degrees (but again for a density smaller than 0.01 particle per cubic meter). The effect on the heat flux is more on the altitude of the reversal than on the amplitude itself, the former getting lower and lower in altitude when the electron precipitation energy increases.

The effect of the total energy E_{tot} is shown only for two values, 5 erg and 100 erg, i.e. a bright aurora and an exceptionally strong one. The shape of the stationary flux does not vary, it is only enhanced. This has no effect on the velocity and on the temperature: the particles are the same, but in larger number. Therefore, the two are indistinguishable in Figure 11. Of course, the more precipitated electrons the more suprathermal ones in the upper atmosphere. This is reflected in the upper left panel (density) where the density reaches 3 particles per cubic meter at 200 km with the highest E_{tot}. The heat flux is also drastically impacted, increasing by a factor of 20 at 225 km.

4 Conclusion

The electron population in the upper atmosphere is divided in a thermal and a suprathermal population. Modelings and measurements of the ionosphere are dealing with the former. The physical characteristics of the latter had never been computed before. This requires several steps: (i) the computation of their distribution function by solving the kinetic Boltzmann equations and (ii) to integrate this function over different power of the velocity. In this work, we provide a solution of this series of integrations up to the power of 3, providing for the suprathermal electrons their density (0th order moment), velocity (1th order moment), temperature (2nd order moment) and heat flux (3rd order moment). Using a kinetic code, we could compute these parameters. We provide a series of results at low latitude over Algiers (Latitude = 36.75°, longitude = 3.04°) at local noon for different solar and geophysical conditions, and at high latitude in the auroral oval above Tromsø (Latitude = 69.58°, longitude = 19.23°) for different precipitation spectra. The main features are:

- The suprathermal density is small compared to the thermal one. Although it is close to 3×10^3 m^{-3} at 180 km (whatever the solar activity) during the day, it drops drastically at night, even under the effect of precipitations, to hardly reach 3 m^{-3}.
- As the density of the electrons increases, they will undergo more elastic and inelastic collisions leading to the decrease of their velocity and temperature.
- Contrarily to the density, the velocity is about 10 times larger during the nighttime when precipitation occur than during the daytime under the electromagnetic solar flux. During the day, its value is negligible at 100 km. It reaches 400,000 m s^{-1} at 200 km whatever the solar and geomagnetic conditions. The increase of the velocity with altitude depends on the solar activity above this altitude. At 400 km, it varies between 700,000 m s^{-1} (active solar conditions) and 900,000 m s^{-1} (quiet Sun). At night, the velocity varies between 3×10^6 m s^{-1} (low mean energy precipitation) and 3×10^7 m s^{-1} (high mean energy precipitation) at 400 km.
- The suprathermal temperature increases as the F10.7 decreases or as the center energy of the electron precipitation increases. It may reach values close to 3×10^8 K, i.e. about 10^5 times larger than that of the thermal electrons.
- The heat flux is hard to be compared to any existing measurement. Depending on the shape of the density, velocity and temperature, it may be fully oriented downward or experience a reversal with some flux going up. In absolute value, its typical upper limit is 2×10^{12} eVm^{-2} s^{-1}) with a maximum between 200 and 300 km depending on the forcing.

These characteristics make their detection a real challenge for the future. Their influences on the usually measured parameters (electron density, temperature, velocity) are dim. The main hope is through the measurement of the plasma line (Guio & Lilensten, 1999). The new EISCAT 3D facility may be a true opportunity for such a challenge.

Acknowledgements. This work was partially funded by the IPEV project on the high latitude polarization of the auroral emissions POLARLIS (project number 1026). It was also funded by the CNRS National solar-terrestrial physics program (PNST). We thank Patrick Guio for helpfull discussions on this topics. We also thank Pr. Mourad Djebli for having made this collaboration possible. The editor thanks Joseph Lemaire and an anonymous reviewer for their assistance in evaluating this paper.

References

Akasofu S-I, Chapman S. 1972. *Solar-terrestrial physics. An account of the wave and particle radiations from the quiet and the active sun, and of the consequent terrestrial phenomena*. International Series of Monographs on Physics. Clarendon Press, Oxford. https://doi.org/10.1007/978-94-009-9519-2

Banks PM, Kockarts G. 1973. Aeronomy. *Springer*. https://doi.org/10.1007/978-82-004-2319-2.

Basu B, Jasperse JR, Strickland DJ, Daniell RE Jr. 1993. Transport-theoretic model for the electron-proton-hydrogen atom aurora. 1: Theory. *J Geophys Res* **98**: 21517–21532. https://doi.org/10.1029/93JA01646.

Bilitza D, Brown SA, Wang MY, Souza JR, Roddy PA. 2012. Measurements and IRI model predictions during the recent solar minimum. *J Atmos Sol-Terr Phys* **86**: 99–106. https://doi.org/10.1016/j.jastp.2012.06.010.

Bittencourt JA, ed. 2010. *Fundamentals of plasma physics*. Springer Verlag. https://doi.org/10.1007/978-1-4757-4030-1.

Blanch E, Altadill D, Juan JM, Camps A, Barbosa J, González-Casado G, Riba J, Sanz J, Vazquez G, Orús-Pérez R. 2018. Improved characterization and modeling of equatorial plasma depletions. *J Space Weather Space Clim* **8**: A38. https://doi.org/10.1051/swsc/2018026.

Blelly PL, Alcaydé D, van Eyken AP. 2010. A new analysis method for determining polar ionosphere and upper atmosphere characteristics from ESR data: Illustration with IPY period. *J Geophys Res (Space Phys)* **115(A9)**: A09,322. https://doi.org/10.1029/2009JA014876.

Culot F, Lathuillère C, Lilensten J. 2005. Influence of geomagnetic activity on the O I 630.0 and 557.7 nm dayglow. *J Geophys Res (Space Phys)* **110**: A01304. https://doi.org/10.1029/2004JA010667.

Guio P, Lilensten J. 1999. Effect of suprathermal electrons on the intensity and Doppler frequency of electron plasma lines. *Ann Geophys* **17(7)**: 903–912. https://doi.org/10.1007/s00585-999-0903-x.

Guio P, Lilensten J, Kofman W, Bjørnå N. 1998. Electron velocity distribution function in a plasma with temperature gradient and in the presence of suprathermal electrons: application to incoherent-scatter plasma lines. *Ann Geophys* **16(10)**: 1226–1240. https://doi.org/10.1007/s00585-998-1226-z.

Hardy DA, Gussenhoven MS, Holeman E. 1985. A statistical model of auroral electron precipitation. *J Geophys Res* **90**: 4229–4248. https://doi.org/10.1029/JA090iA05p04229.

Jasperse JR. 1976. Boltzmann-Fokker-Planck model for the electron distribution function in the Earth's ionosphere. *Planet Space Sci* **24(1)**: 33–40. https://doi.org/10.1016/0032-0633(76)90058-1.

Jin Y, Miloch WJ, Moen JI, Clausen LBN. 2018. Solar cycle and seasonal variations of the GPS phase scintillation at high latitudes. *J Space Weather Space Clim* **8**: A48. https://doi.org/10.1051/swsc/2018034.

Kelley M. 2009. *The Earth's ionosphere*, vol. 96 of International Geophysics Series. Elsevier Academic, ISBN 978-0-12-088425-4.

Kofman W, St-Maurice JP, van Eyken AP. 1993. Heat flow effect on the plasma line frequency. *J Geophys Res* **98(A4)**: 6079–6086. https://doi.org/10.1029/92JA02703.

Lilensten J, Blelly PL. 2000. *Du soleil a la terre*, ISBN 2-7061-0834-7. collection. Grenoble Sciences, EDP Sciences, ISBN 978-2-86883-467-6.

Lilensten J, Blelly PL. 2002. The TEC and F2 parameters as tracers of the ionosphere and thermosphere. *J Atmos Terr Phys* **64**: 775–793. https://doi.org/10.1016/S1364-6826(02)00079-2.

Lilensten J, Cander LR. 2003. Calibration of the TEC derived from GPS measurements and from ionospheric models using the EISCAT radar. *J Atmos Sol Terr Phys* **65**: 833–842. https://doi.org/10.1016/S1364-6826(03)00087-7.

Lilensten J, Simon Wedlund C, Barthélémy M, Thissen R, Ehrenreich D, Gronoff G, Witasse O. 2013. Dications and thermal ions in planetary atmospheric escape. *Icarus* **222**: 169–187. https://doi.org/10.1051/swsc/2012023.

Lummerzheim D, Lilensten J. 1994. Electron transport and energy degradation in the ionosphere: Evaluation of the numerical solution, comparison with laboratory experiments and auroral observations. *Ann Geophys* **12**: 1039–1051. https://doi.org/10.1007/s00585-994-1039-7.

Lummerzheim D, Rees MH, Anderson HR. 1989. Angular dependent transport of auroral electrons in the upper atmosphere. *Planet Space Sci* **37**: 109–129. https://doi.org/10.1016/0032-0633(89)90074-3.

Mantas GP. 1975. Theory of photoelectron thermalization and transport in the ionosphere. *Planet Space Sci* **23**: 337–354. https://doi.org/10.1016/0032-0633(75)90139-7.

Min QL, Lummerzheim D, Rees MH, Stamnes K. 1993. Effects of a parallel electric field and the geomagnetic field in the topside ionosphere on auroral and photoelectron energy distributions. *J Geophys Res* **98**: 19223–19234. https://doi.org/10.1029/93JA01742.

Opal C, Peterson W, Beaty E. 1971. Measurements of secondary-electron spectra produced by electron impact ionization of a number of simple gases. *J Chem Phys* **55**: 4100. https://doi.org/10.1063/1.1676707.

Picone JM, Hedin AE, Drob DP, Aikin AC. 2002. NRLMSISE-00 empirical model of the atmosphere: Statistical comparisons and scientific issues. *J Geophys Res (Space Phys)* **107**: 1468. https://doi.org/10.1029/2002JA009430.

Pitout Blelly, Alcaydà Pitout F, Blelly PL, Alcaydé D. 2013. High-latitude ionospheric response to the solar eclipse of 1 August 2008: EISCAT observations and TRANSCAR simulation. *J Atmos Sol Terr Phys* **105**: 336–349. https://doi.org/10.1016/j.jastp.2013.02.004.

Rees MH. 1989. *Physics and chemistry of the upper atmosphere*. University Press, Cambridge. ISBN 0521368480. ISBN 0-521-32305-3.

Schunk RW, Nagy AF. 2000. *Ionospheres*. Cambridge University Press, ISBN 0-521-63237-4.

Stamnes K, Tsay SC, Wiscombe WJ, Jayaweera K. 1988. Numerically stable algorithm forDiscrete-Ordinate-Method radiative transfer in a multiple scattering and emitting layered media. *Appl Opt* **27**: 2502. https://doi.org/10.1364/AO.27.002502.

Strickland DJ, Book DL, Coffey TP, Fedder JA. 1976. Transport equation technique for the deposition of auroral electrons. *J Geophys Res* **81**: 2755. https://doi.org/10.1029/JA081i016p02755.

Swartz WE. 1985. Optimization of energetic electron energy degradation calculations. *J Geophys Res* **90**: 6587. https://doi.org/10.1029/JA090iA07p06587.

Swartz WE, Nisbet JS. 1972. Revised calculations of the F-region ambiant electron heating by photoelectrons. *J Geophys Res* **77**: 6259. https://doi.org/10.1029/JA077i031p06259.

Woods LC. 1993. *An introduction to the kinetic theory of gases and magnetoplasmas*. Oxford Science Publications. https://doi.org/10.1017/S0022112095220780.

Woods TN, Chamberlin PC, Harder JW, Hock RA, Snow M, Eparvier FG, Fontenla J, McClintock WE, Richard EC. 2009. Solar Irradiance Reference Spectra (SIRS) for the 2008 Whole Heliosphere Interval (WHI). *Geophys Res Lett* **36(1)**: L01101. https://doi.org/10.1029/2008GL036373.

Appendix A

Computation of the suprathermal electron moments: first demonstration

A.1 From f to ϕ

Classically, the Boltzmann distribution function (in cm^{-6} s^3) is $f(t,\vec{r},\vec{v})$.The velocity of the particle is $\vec{v}$ which is splitted in velocities parallel and perpendicular to the magnetic field line:

$$\vec{v} = v_{//}\vec{i_{//}} + v_{\perp}\vec{i_{\perp}} \tag{A.1}$$

where $\vec{i_{//}}$ and $\vec{i_{\perp}}$ are the unitary vectors along the magnetic field line and perpendicular. We make the stationary hypothesis so that there is no time anymore to consider. The electrons are gyrating along the magnetic field that we call the z axis, so that the Boltzmann distribution function can be simply expressed as $f(z, v_{\perp},v_{//})$.

We call θ the angle between the magnetic field line and the electron velocity vector (usually also called "pitch angle") and $\mu = \cos(\theta)$, so that:

$$\begin{cases} v_{\perp} = |\vec{v}|\sin\theta = |\vec{v}|\sqrt{1-\mu^2} \\ v_{//} = |\vec{v}|\cos\theta = |\vec{v}|\mu \end{cases} \tag{A.2}$$

Since the electrons are not relativistic, their kinetic energy writes $E = \frac{1}{2}mv^2$ so that we can write:

$$\begin{cases} |\vec{v}| = \sqrt{\frac{2E}{m}} \\ v_{\perp} = \sqrt{\frac{2E}{m}}\sqrt{1-\mu^2} \\ v_{//} = \sqrt{\frac{2E}{m}}\mu \end{cases} \tag{A.3}$$

In cylindric coordinates (Fig. A.1), a volume element writes $d\Omega = r{\cdot}dr{\cdot}d\theta{\cdot}d\phi$. In the $(\vec{i_{//}}, \vec{i_{\perp}})$ system, the full rotation of ϕ is 2π and the volume element writes:

$$d\Omega = 2\pi v_{\perp}dv_{\perp}dv_{//}. \tag{A.4}$$

We want to write this volume element in the new frame E, μ where we aim at writing the new distribution function $\phi(z, E, \mu)$ in cm^{-2} eV^{-1} s^{-1} sr^{-1}. To do so, we need to express the volume element in the two frames:

$$d\Omega = 2\pi\, v_{\perp}dv_{\perp}dv_{//} = 2\pi\det(J)\,d\mu\,dE \tag{A.5}$$

where J is the Jacobian:

$$J = \begin{pmatrix} \frac{dv_{//}}{d\mu} & \frac{dv_{//}}{dE} \\ v_{\perp}\frac{dv_{\perp}}{d\mu} & v_{\perp}\frac{dv_{\perp}}{dE} \end{pmatrix}. \tag{A.6}$$

From equation (A.2) we find:

$$J = \begin{pmatrix} \sqrt{\frac{2E}{m}} & \frac{\mu}{\sqrt{2mE}} \\ \frac{-2\mu E}{m} & \frac{1-\mu^2}{m} \end{pmatrix}. \tag{A.7}$$

Introducing the determinant of J in equation (B.7) we get:

$$d\Omega = 2\pi\, v_{\perp}dv_{\perp}dv_{//} = 2\pi\sqrt{\frac{2E}{m^3}}\,d\mu\,dE. \tag{A.8}$$

The element flux dF of electrons along B can be written in the two systems:

$$\begin{cases} dF = \vec{v}f(\vec{r},\vec{v})d\Omega = |\vec{v}|\,f(z,v_{\perp},v_{//})2\pi\, v_{\perp}dv_{\perp}dv_{//} \\ dF = \phi(z,E,\mu)2\pi\,d\mu\,dE \end{cases} \tag{A.9}$$

Using equation (A.8) and the value of the velocity versus energy, one gets:

$$f(z,v_{\perp},v_{//}) = \frac{m^2}{2E}\phi(z,E,\mu). \tag{A.10}$$

A.2 Moments

A.2.1 Zeroth order moment: the supra thermal electron density

In Boltzmann's formalism, the density $n(z)$ (in cm^{-3}) is:

$$n(z) = \int f(z,v)dv \tag{A.11}$$

which becomes here:

$$n(z) = \int f(z,v_{\perp},v_{//})2\pi\, v_{\perp}dv_{\perp}dv_{//} \tag{A.12}$$

or, replacing f with its value in (A.10) and the integrands with their values in (A.8):

$$n(z) = 2\pi\iint\sqrt{\frac{m}{2E}}\phi(z,E,\mu)\,d\mu\,dE. \tag{A.13}$$

We can now compute the average $\langle X\rangle$ of any random variable X as:

$$\langle X\rangle = \frac{1}{n(z)}\int Xf(z,v_{\perp},v_{//})\,2\pi\, v_{\perp}dv_{\perp}dv_{//} \tag{A.14}$$

and transform it in the (μ, E) frame using exactly the same method.

A.2.2 First order moment: the supra thermal electron velocity

The second moment is the velocity (in cm s^{-1}). It is important to note that around a full rotation, the average of the perpendicular velocity is null, so that $\langle v\rangle = \langle v_{//}\rangle$:

$$\langle v\rangle = \langle v_{//}\rangle = \frac{1}{n(z)}\int v_{//}f(z,v_{\perp},v_{//})2\pi\, v_{\perp}dv_{\perp}dv_{//} \tag{A.15}$$

becomes:

$$\langle v\rangle = \langle v_{//}\rangle = 2\pi\frac{1}{n(z)}\iint\phi(z,E,\mu)\,\mu\,d\mu\,dE. \tag{A.16}$$

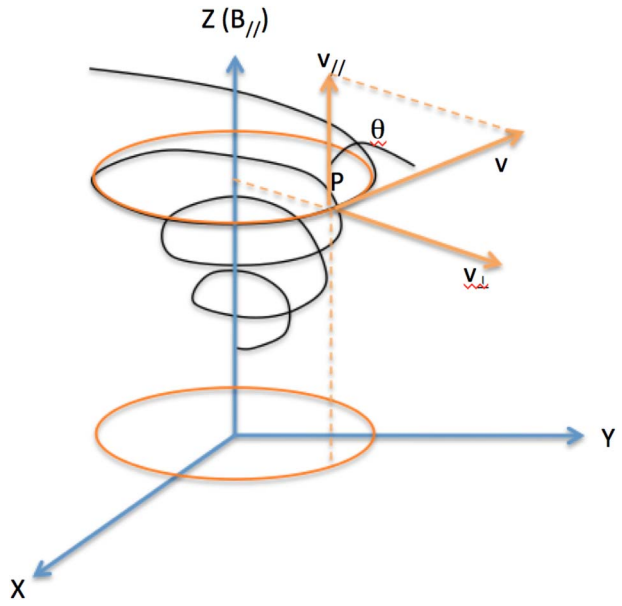

Fig. A.1. Usual cylindric coordinates. The electron follows a spiral around the magnetic field, taken as the z axis. The projection of its velocity on this axis is $v_{\|}$. The projection on the perpendicular plane is $v_{\perp}$.

A.2.3 Second order moment: the supra thermal electron temperature

To compute the suprathermal electron temperature (in K), we use the thermodynamic definition of the kinetic temperature $\frac{3}{2}kT = \frac{1}{2}m\langle c^2\rangle$ where k is of the Boltzmann constant and $\vec{c}$ is the difference between the instantaneous velocity $\vec{v}$ and its average (mean) $\langle\vec{v}\rangle$. Note that we consider these electrons as having three degrees of freedom while the thermal ones usually have only two. The reason is that the thermal ones are constrained along the magnetic field while the suprathermal are created in any pitch angle:

$$\vec{c} = \vec{v} - \langle\vec{v}\rangle. \tag{A.17}$$

So

$$\frac{3}{2}kT = \frac{1}{2}m\left(\langle v^2\rangle - \langle v\rangle^2\right). \tag{A.18}$$

So that

$$\frac{3}{2}kT = \frac{m}{2n(z)}\int v^2 f(z, v_{\perp}, v_{//}) 2\pi\, v_{\perp} \mathrm{d}v_{\perp}\mathrm{d}v_{//} - \frac{m\langle v\rangle^2}{2} \tag{A.19}$$

which becomes:

$$\frac{3}{2}kT = 2\pi\frac{1}{n(z)}\iint\sqrt{\frac{mE}{2}}\phi(z, E, \mu)\,\mathrm{d}\mu\,\mathrm{d}E - \frac{m\langle v\rangle^2}{2}. \tag{A.20}$$

This allow to define the total temperature T_{tot} in relation to the instantaneous velocity v, defined by:

$$T_{\mathrm{tot}} = \frac{2\pi}{3k}\frac{1}{n(z)}\iint\sqrt{2mE}\;\phi(z, E, \mu)\;\mathrm{d}\mu\;\mathrm{d}E. \tag{A.21}$$

Which can be written according to equation (A.20) as:

$$T_{\mathrm{tot}} = \frac{3}{2}kT + \frac{m\langle v\rangle^2}{2}. \tag{A.22}$$

It is the sum of two components because the velocity of the electrons may be divided in the mean velocity along B computed in equation (A.16) (again, the perpendicular velocity average is null) and the specific fluctuation of the velocity $\vec{c}$ depending on each electron agitating energy with the corresponding kinetic or specific temperature T_{spec}. The mean temperature due to the mean velocity is simply:

$$T_{\mathrm{mean}} = \frac{m\langle v_{//}\rangle^2}{3k} \tag{A.23}$$

and we get:

$$T_{\mathrm{spec}} = \frac{2\pi}{3k}\frac{1}{n(z)}\iint\sqrt{2mE}\;\phi(z, E, \mu)\,\mathrm{d}\mu\,\mathrm{d}E - \frac{m\langle v_{//}\rangle^2}{3k}. \tag{A.24}$$

A.2.4 Third order moment: the supra thermal electron heat flow

The heat flow, in eV cm^{-2} s^{-1} writes:

$$\vec{q}(z) = \frac{1}{2}n(z)mc^2\vec{c}. \tag{A.25}$$

Since the mean velocity is only carried by the parallel axis, $\vec{c}$ can also be written:

$$\vec{c} = \begin{pmatrix} v_{//} - \langle v\rangle \\ v_{\perp}\end{pmatrix}. \tag{A.26}$$

So that

$$c\cdot c = \begin{pmatrix} v_{//} - \langle v\rangle \\ v_{\perp}\end{pmatrix}(v_{//} - \langle v\rangle\; v_{\perp}) \tag{A.27}$$

which develops in:

$$c\cdot c = v_{//}^2 + \langle v\rangle^2 - 2\langle v\rangle v_{//} + v_{\perp}^2 \tag{A.28}$$

But, $v^2 = v_{//}^2 + v_{\perp}^2$ so that equation (A.28) becomes more simply:

$$c\cdot c = v^2 + \langle v\rangle^2 - 2\langle v\rangle v_{//} \tag{A.29}$$

and the components of $c\cdot c\cdot\vec{c}$ are:

$$cc\,\vec{c} = \begin{pmatrix} (v^2 + \langle v\rangle^2 - 2\langle v\rangle v_{//})(v_{//} - \langle v\rangle) \\ (v^2 + \langle v\rangle^2 - 2\langle v\rangle v_{//})v_{\perp}\end{pmatrix}. \tag{A.30}$$

Since we are going to make a mean by integrating on the Boltzmann function and $\langle v_{\perp}\rangle = 0$, the heat flow is along the parallel axis only. Its value is then:

$$q_{//}(z) = \frac{1}{2}n(z)m(v^2 + \langle v\rangle^2 - 2\langle v\rangle v_{//})(v_{//} - \langle v\rangle). \tag{A.31}$$

We develop it to get:

$$q_{//}(z) = \frac{1}{2}n(z)m(v^2 v_{//} + v^2\langle v\rangle + 3\langle v\rangle^2 v_{//} - \langle v\rangle^3 - 2\langle v\rangle v_{//}^2). \tag{A.32}$$

In this equation, the different velocities can be expressed in term of the energy E, the cosine of the pitch angle μ and the mass m through the set of equations (A.33)

$$q_{//}(z) = \frac{1}{2} n(z) m \left(\frac{2E}{m} \sqrt{\frac{2E}{m}} \mu - \frac{2E}{m} \langle v \rangle + 3 \langle v \rangle^2 \sqrt{\frac{2E}{m}} \mu - \langle v \rangle^3 - 2 \langle v \rangle \frac{2E}{m} \mu^2 \right). \quad \text{(A.33)}$$

This can be written as the sum of 5 heat flow components $q_{//}(z) = q_1(z) + q_2(z) + q_3(z) + q_4(z) + q_5(z)$, each of them having to be averaged as in equation (A.14)

$$\chi_i(z) = \frac{1}{n(z)} \int q_i(z) f(z, v_\perp, v_{//}) 2\pi v_\perp \mathrm{d}v_\perp \mathrm{d}v_{//}. \quad \text{(A.34)}$$

As above, we use equations (A.8) and (A.10) to write this series of integrals as:

$$\chi_i(z) = \frac{1}{n(z)} \int q_i(z) \frac{m^2}{2E} 2\pi \sqrt{\frac{2E}{m^3}} \phi(z, E, \mu) \, \mathrm{d}\mu \, \mathrm{d}E. \quad \text{(A.35)}$$

The stationary electron flux $\phi(z, E, \mu)$ is integrated over $\mathrm{d}\mu$ in χ_2 and χ_4, over $\mu \mathrm{d}\mu$ in χ_1 and χ_3 and finally over $\mu^2 \mathrm{d}\mu$ in χ_5. Lets call $\phi_j(z, E)$ these integrals:

$$\phi_j(z, E) = 2\pi \int \mu^j \phi(z, E, \mu) \, \mathrm{d}\mu. \quad \text{(A.36)}$$

We now replace successively the five values of q_i given (Eq. (A.32)) in equation (A.35). After some basics algebra, we obtain $\chi(z) = \chi_1(z) + \chi_2(z) + \chi_3(z) + \chi_4(z) + \chi_5(z)$ where:

$$\begin{cases} \chi_1(z) = \int E \phi_1(z, E) \ \mathrm{d}E \\ \chi_2(z) = -\langle v \rangle \int \phi_0(z, E) \sqrt{\frac{mE}{2}} \ \mathrm{d}E \\ \chi_3(z) = \frac{3}{2} m \langle v \rangle^2 \int \phi_1(z, E) \ \mathrm{d}E \\ \chi_4(z) = -\langle v \rangle^3 \sqrt{\frac{m^3}{8}} \int \frac{1}{\sqrt{E}} \phi_0(z, E) \ \mathrm{d}E \\ \chi_5(z) = -\langle v \rangle \int \phi_2(z, E) \sqrt{2mE} \ \mathrm{d}E \end{cases} \quad \text{(A.37)}$$

Appendix B

B Computation of the suprathermal electron moments: second demonstration

B.1 From f to ϕ

The electrons are gyrating along the magnetic field that we call the z axis (Fig. A.1). Usually, moments are systematically deduced from knowledge of the distribution function $f(t, \vec{r}, \vec{v})$ (in $\mathrm{cm}^{-6}\ \mathrm{s}^3$). In this work, The suprathermal elctron moments are calculated in term of the suprathermal electron flux $\phi(z, E, \mu)$ (in $\mathrm{cm}^{-2}\ \mathrm{eV}^{-1}\ \mathrm{s}^{-1}\ \mathrm{sr}^{-1}$), solution of the electron Boltzmann kinetic equation. For this purpose, we will first find the relationship between the classical distribution function $f(t, \vec{r}, \vec{v})$ and the electron flux $\phi(t, \vec{r}, E, \vec{\Omega})$ at the position $\vec{r}$, with the energy E at the direction $\vec{\Omega} = \frac{\vec{v}}{v}$.

$vf(t, \vec{r}, \vec{v})$ is the electron flux of velocity $\vec{v}$ at the direction $\vec{\Omega} = \frac{\vec{v}}{v}$. So:

$$vf(t, \vec{r}, \vec{v}) \, \mathrm{d}\vec{v} = \phi\left(t, \vec{r}, E, \vec{\Omega}\right) \mathrm{d}E \, \mathrm{d}\vec{\Omega}. \quad \text{(B.1)}$$

For non-relativistic electrons, the kinetic energy writes $E = \frac{1}{2} m v^2$ which gives $\mathrm{d}E = mv\mathrm{d}v$.

We consider a spherical polar coordinate system in velocity space (v, θ, ϕ) (Fig. B.1). A volume element writes:

$$\mathrm{d}\vec{v} = v^2 \sin(\theta) \ \mathrm{d}v \ \mathrm{d}\theta \ \mathrm{d}\phi \quad \text{(B.2)}$$

where θ is the angle between v_z and the electron velocity vector (usually also called "pitch angle") and $\mu = \cos(\theta)$.

The above makes it possible to write:

$$\frac{\mathrm{d}\vec{v}}{\mathrm{d}v} = v^2 \sin(\theta) \, \mathrm{d}\theta \ \mathrm{d}\phi. \quad \text{(B.3)}$$

A surface element $\mathrm{d}\vec{s}$ in the velocity space swept by the vector $\mathrm{d}\vec{\Omega}$ of electrons of velocity $\mathrm{d}\vec{v}$ is given by:

$$\mathrm{d}\vec{s} = v^2 \mathrm{d}\vec{\Omega}. \quad \text{(B.4)}$$

But in spherical coordinates (Fig. B.1), a surface element writes:

$$\mathrm{d}\vec{s} = v^2 \sin(\theta) \, \mathrm{d}\theta \ \mathrm{d}\phi. \quad \text{(B.5)}$$

Using equations (B.3) and (B.4) we get:

$$\mathrm{d}\vec{s} = \frac{\mathrm{d}\vec{v}}{\mathrm{d}v} = v^2 \sin(\theta) \ \mathrm{d}\theta \ \mathrm{d}\phi \quad \text{(B.6)}$$

and

$$\mathrm{d}\Omega = \sin(\theta) \ \mathrm{d}\theta \ \mathrm{d}\phi. \quad \text{(B.7)}$$

Including equation $\mathrm{d}\vec{\Omega}$ in equation (B.1) we get:

$$f(t, \vec{r}, \vec{v}) \ \mathrm{d}\vec{v} = \frac{1}{v} \phi\left(t, \vec{r}, E, \vec{\Omega}\right) \mathrm{d}E \sin(\theta) \ \mathrm{d}\theta \ \mathrm{d}\phi. \quad \text{(B.8)}$$

Combining equations (B.6) and (B.8) and the value of $\mathrm{d}E$ versus $\mathrm{d}v$, we can write:

$$\frac{v^2}{m} f(t, \vec{r}, \vec{v}) = \phi(t, \vec{r}, E, \vec{\Omega}) \quad \text{(B.9)}$$

or

$$f(t, \vec{r}, \vec{v}) = \frac{m^2}{2E} \phi\left(t, \vec{r}, E, \vec{\Omega}\right). \quad \text{(B.10)}$$

We make the stationary hypothesis and take into account that the electrons are gyrating in the configuration space along the magnetic field lines that we call the z axis. The Boltzmann distribution function can simply be expressed as $f(z, \vec{v})$.

Using the value of θ versus μ, one gets:

$$f(z, \vec{v}) \ \mathrm{d}\vec{v} = \frac{1}{v} \ \phi(z, E, \mu) \ \mathrm{d}E \ \mathrm{d}\mu \ \mathrm{d}\phi = \sqrt{\frac{m}{2E}} \ \phi(z, E, \mu) \ \mathrm{d}E \ \mathrm{d}\mu \ \mathrm{d}\phi \quad \text{(B.11)}$$

and

$$f(z, \vec{v}) = \frac{m}{v^2} \ \phi(z, E, \mu) = \frac{m^2}{2E} \ \phi(z, E, \mu). \quad \text{(B.12)}$$

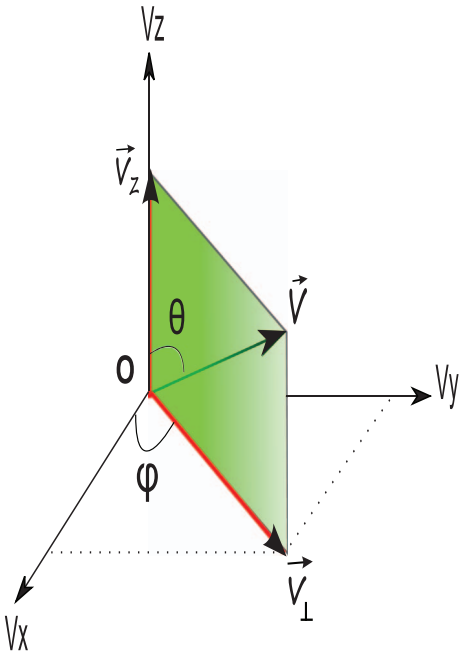

Fig. B.1. Spherical coordinate system (v, θ, ϕ) in the velocity space. The Vz axis is in the direction of the local magnetic field B.

B.2 Momentums

B.2.1 Zeroth order moment: the supra thermal electron density

In Boltzmann's formalism, the density $n(z)$ (in cm^{-3}) is given by:

$$n(z) = \int f(z, \vec{v}) \mathrm{d}\vec{v}. \tag{B.13}$$

Using equation (B.11) it becomes:

$$\begin{aligned} n(z) &= \int \frac{1}{v}\, \phi(z, E, \mu)\, \mathrm{d}E\, \mathrm{d}\mu\, \mathrm{d}\phi \\ &= \int \sqrt{\frac{m}{2E}}\, \phi(z, E, \mu)\, \mathrm{d}E\, \mathrm{d}\mu\, \mathrm{d}\phi. \end{aligned} \tag{B.14}$$

In the spherical coordinate system (v, θ, ϕ) (Fig. B.1), the full rotation of ϕ is 2π. The density writes:

$$n(z) = 2\pi \iint \sqrt{\frac{m}{2E}}\, \phi(z, E, \mu)\, \mathrm{d}\mu\, \mathrm{d}E. \tag{B.15}$$

The average $\langle X \rangle$ of any random variable X can then be computed as:

$$\langle X \rangle = \frac{1}{n(z)} \int X f(z, \vec{v})\, \mathrm{d}\vec{v}. \tag{B.16}$$

In the (z, E, μ) frame, $\langle X \rangle$writes:

$$\begin{aligned} \langle X \rangle &= \frac{2\pi}{n(z)} \iint \frac{1}{v}\, X \phi(z, E, \mu)\, \mathrm{d}\mu\, \mathrm{d}E \\ &= \frac{2\pi}{n(z)} \iint \sqrt{\frac{m}{2E}}\, X \phi(z, E, \mu)\, \mathrm{d}\mu\, \mathrm{d}E. \end{aligned} \tag{B.17}$$

B.2.2 First order moment: the supra thermal electron velocity

The second moment is the velocity v (in cm s^{-1}).

The velocity vector $\vec{v}$ of the electron can be splitted into a component $\vec{v_z}$ parallel to the magnetic field line (i.e. to Vz axis) and another one $\vec{v_\perp}$ perpendicular to the magnetic field line and situated in the plane (Vx, Vy) (Fig. B.1):

$$\vec{v} = \vec{v_z} + \vec{v_\perp}. \tag{B.18}$$

Such as:

$$\begin{cases} v &= \sqrt{\frac{2E}{m}} \\ v_z &= v \cos\theta = v\mu \\ v_\perp &= v \sin\theta = v\sqrt{1-\mu^2} \end{cases}. \tag{B.19}$$

It is important to note that around a full rotation, the average of the perpendicular velocity is null, so that $\langle v \rangle = \langle v_z \rangle$.

Equations (B.17) and (B.19) allow to write the average velocity in the form:

$$v = v_z = \frac{2\pi}{n(z)} \iint \phi(z, E, \mu)\, \mu\, \mathrm{d}\mu\, \mathrm{d}E \tag{B.20}$$

B.2.3 Second order moment: the supra thermal electron temperature

To compute the suprathermal electron temperature (in K), we use the thermodynamic definition of the kinetic temperature:

$$\frac{3}{2} kT = \frac{1}{2} mc^2 \tag{B.21}$$

where k is the Boltzmann constant and $\vec{c}$ is the random or specific velocity defined as the velocity of the electron relative to the average (mean) velocity $\langle \vec{v} \rangle$:

$$\vec{c} = \vec{v} - \langle \vec{v} \rangle \tag{B.22}$$

so

$$\frac{3}{2} kT = \frac{1}{2} m \left(\langle v^2 \rangle - \langle v \rangle^2 \right). \tag{B.23}$$

So that

$$\frac{3}{2} kT = \frac{m}{2n(z)} \int v^2 f(z, \vec{v})\, \mathrm{d}\vec{v} - \frac{m \langle v \rangle^2}{2} \tag{B.24}$$

which becomes:

$$3kT = \frac{2\pi m}{n(z)} \iint v \phi(z, E, \mu)\, \mathrm{d}\mu\, \mathrm{d}E - m \langle v \rangle^2. \tag{B.25}$$

This allow to define the total temperature T_{tot} in relation to the instantaneous velocity v, defined by:

$$T_{\mathrm{tot}} = \frac{2\pi}{3k} \frac{1}{n(z)} \iint \sqrt{2mE}\, \phi(z, E, \mu)\, \mathrm{d}\mu\, \mathrm{d}E. \tag{B.26}$$

Which can be written according to equation (B.25) as:

$$T_{\mathrm{tot}} = \frac{3}{2} kT + \frac{m \langle v \rangle^2}{2}. \tag{B.27}$$

It is the sum of two components because the velocity of the electrons may be divided in the mean velocity along B computed in equation (B.20) and the specific fluctuation of the velocity $\vec{c}$ depending on each electron agitating energy with the corresponding kinetic or specific temperature T_{spec}. The mean temperature due to the mean velocity is simply:

$$T_{\text{mean}} = \frac{m\langle v\rangle^2}{3k} = \frac{m\langle v_z\rangle^2}{3k}. \tag{B.28}$$

And we get:

$$T_{\text{spec}} = \frac{2\pi}{3k}\frac{1}{n(z)}\iint \sqrt{2mE}\;\; \phi(z,E,\mu)\,\mathrm{d}\mu\,\mathrm{d}E - \frac{m\langle v_z\rangle^2}{3k} \tag{B.29}$$

B.2.4 Third order moment: the supra thermal electron heat flow

The demonstration reads as in Section A.2.4. However, we can easily notice that using equation (B.20), $\chi_3(z)$ in equation (A.37) can be written as:

$$\chi_3(z) = \frac{3}{2}mn\langle v\rangle^3. \tag{B.30}$$

Likewise, using equation (B.15), $\chi_4(z)$ in equation (A.37) can be written as:

$$\chi_4(z) = -\frac{1}{2}mn\,\langle v\rangle^3. \tag{B.31}$$

Equations (B.30) and (B.31) make it possible to write:

$$\chi_{34}(z) = \chi_3(z) + \chi_4(z) = mn\,\langle v\rangle^3. \tag{B.32}$$

The heat flow can then be written as the sum of 4 heat flow components:

$$\chi(z) = \chi_1(z) + \chi_2(z) + \chi_{34}(z) + \chi_5(z) \tag{B.33}$$

where

$$\begin{cases} \chi_1(z) = \int E\phi_1(z,E)\;\;\mathrm{d}E \\ \chi_2(z) = -\langle v\rangle \int \phi_0(z,E)\sqrt{\frac{mE}{2}}\;\;\mathrm{d}E \\ \chi_{34}(z) = mn\,\langle v\rangle^3 \\ \chi_5(z) = -\langle v\rangle \int \phi_2(z,E)\sqrt{2mE}\;\;\mathrm{d}E \end{cases} \tag{B.34}$$

and $\phi_j(z,E) = 2\pi\int \mu^j\phi(z,E,\mu)\;\mathrm{d}\mu$ for j = 0, 1 or 2.

Cite this article as: Marif H & Lilensten J 2020. Suprathermal electron moments in the ionosphere. *J. Space Weather Space Clim.* **10**, 22.